

# Theoretical Modeling of Ground Motion

by

**Shahram Pezeshk, Ph.D., P.E.**

*Department of Civil Engineering*

*The University of Memphis*

*Memphis, TN 38152*

# Chapter 2

## Theoretical Modeling of Ground Motion

### 2.1 Introduction

#### 2.1.1 Background

West Tennessee is located in the central United States and is close to the New Madrid seismic source zone (NMSZ). Though 1811-12 great New Madrid earthquakes occurred in the NMSZ, the number of strong earthquakes in the NMSZ is much less than in the western United States. Especially, there is lack of earthquakes with strong ground motion recordings in the central United States. Therefore, it is impossible to obtain a strong ground motion attenuation function by statistical analysis of available ground motion recordings for the NMSZ. To meet the need of earthquake resistant design, ground motion in the NMSZ is usually estimated by the stochastic-point-source model.

The stochastic-point-source model was proposed in the seventies. To overcome the deficiency of strong ground motion recordings, Hanks (1979), McGuire and Hanks (1980), and Hanks and McGuire (1981) developed a method for estimating peak ground motion parameters on the basis of seismological theory. They treated the ground motion as *band-limited*<sup>[1]</sup> *finite-duration*<sup>[2]</sup> *stationary*<sup>[3]</sup> *Gaussian*<sup>[4]</sup> *white noise*<sup>[5]</sup>, with a source spectrum given by Brune's (1970,1971) omega square model for far-field shear radiation. Hanks and McGuire (1981) used Parseval's theorem to predict the root-mean-square (rms) acceleration ( $a_{rms}$ ) from the integral of the squared acceleration spectrum; then they used random vibration theory to relate the  $a_{rms}$  to PGA. The model was later extended by Boore (1983) and McGuire et al. (1984) to predict PGV and pseudo response spectral values.

---

\* Italic words are explained in the Glossary

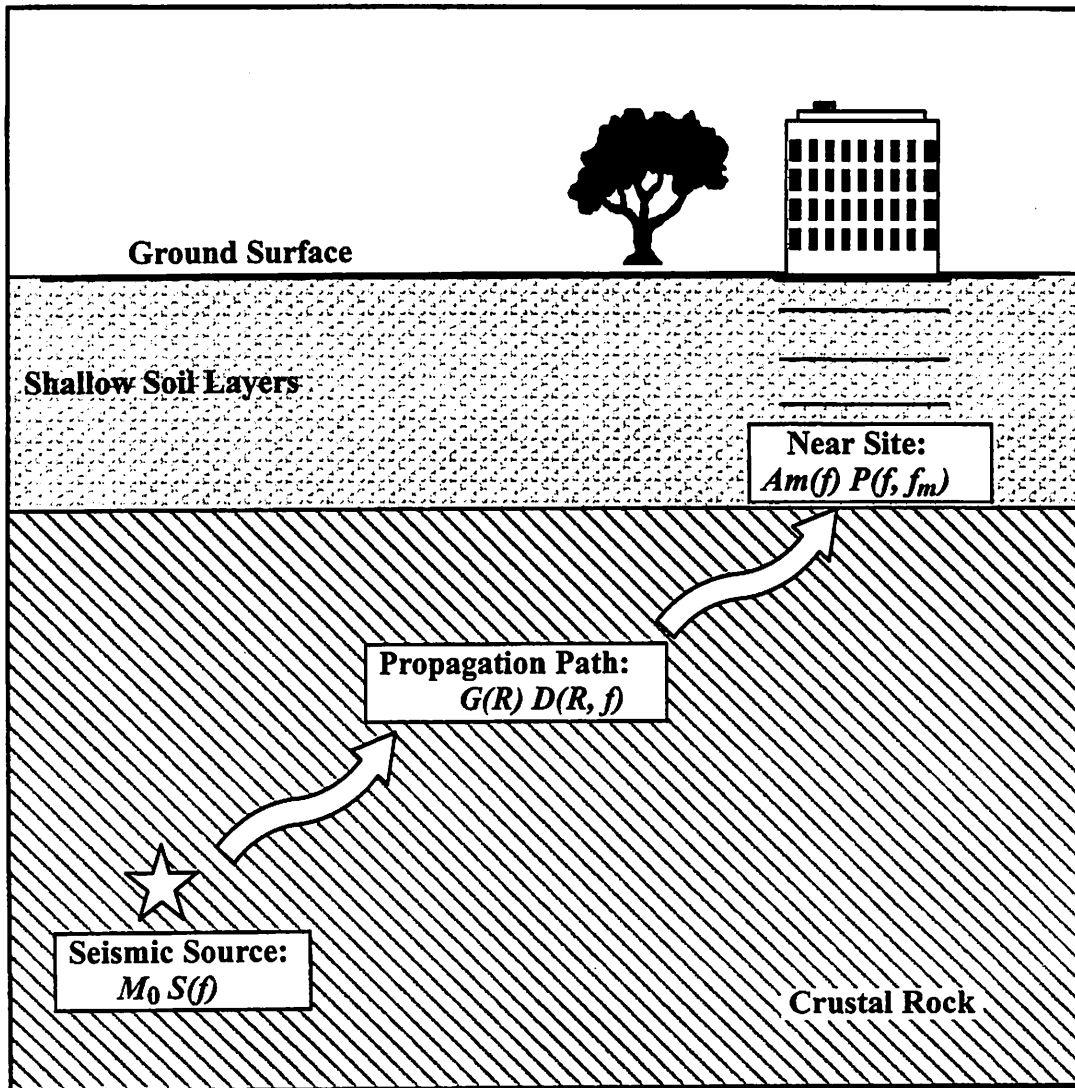


*Figure 2.1. Factors that Affect the Estimation of Ground Motions at a Site of Interest.*

where  $R_{\theta\phi}$  is the average radiation pattern corresponding to different types of seismic waves over a range of azimuths  $\theta$  and take-off angles  $\phi$ . Boore and Boatwright (1984) found the shear-wave radiation pattern  $R_{\theta\phi}$  is 0.55 for  $\phi$  and  $\theta$  average over the whole focal sphere;  $F$  is the free surface amplification and is usually taken as 2;  $V$  is the factor considering the seismic energy partition onto horizontal components and  $1/\sqrt{2}$  is used by most researchers;  $\rho$  is the density and  $\beta$  is the shear wave velocity at focal depth;  $S(f)$  is the seismic source spectral shape;  $G(R)$  is the geometric attenuation of seismic wave;  $D(R, f)$  is the inelastic

Compared with the time domain simulation, the estimation of response spectra from RVT is not as good as that of peak ground motion (Boore, 1983; Boore and Joyner, 1984). In recent years, instead of the RVT method, the time domain simulation (TDS) is used to estimate peak amplitude values and response spectral values in the application (EPRI, 1993; Boore et al., 1996). To improve the estimation of spectral values, we propose two new methods for estimating the pseudo spectral velocity or acceleration in the frequency domain. Then we compare our results with those from TDS and previous research.

## 2.2 Fourier Amplitude Spectra

Concepts behind the stochastic-point-source model are illustrated graphically in Figure 2.1. Following Aki and Richards (1980), McGuire and Hanks (1980), Herrmann and Kijko (1983), and Boore (1983), the Fourier amplitude spectrum,  $A(M_0, R, f)$ , of ground acceleration at rock site can be expressed by

$$A(M_0, R, f) = C M_0 \times S(f) \times G(R) \times D(R, f) \times Am(f) \times P(f, f_m) \quad (2.1)$$

where  $R$  is the hypocentral distance (Pezeshk et al., 1996),  $f$  is the frequency of seismic wave, and  $M_0$  is the seismic moment generated by the earthquake which can be calculated according to the seismic moment and moment magnitude relationship developed by Hanks and Kanamori (1979)

$$\log(M_0) = 1.5M + 16.1 \quad (2.2)$$

where  $M$  is the moment magnitude.

The parameter  $C$  is the seismic source scaling factor, given by the formula

$$C = \frac{R_{\theta\phi} FV}{4\pi\varrho\beta^3} \quad (2.3)$$

attenuation of seismic wave;  $Am(f)$  is the amplification factor due to the difference of properties ( $\rho$  and  $\beta$ ) between rock at focal depth and beneath the site or surface;  $P(f, f_m)$  is the high-cut filter or near-site attenuation; and  $f_m$  is the high cutoff frequency.

From Equation (2.1), it is clear that this model is quite simple and effects of the seismic source, the wave propagation path, and the local geology are naturally separated. As a result, it is possible to individually quantify these influences.

## 2.3 Quantification of Seismic Source

Basically, there are four main parameters to define seismic source for the estimation of ground motion. They are the earthquake magnitude, the focal depth, the source spectral shape, and the stress drop (Pezeshk et al., 1996).

### 2.3.1 Magnitude

The magnitude is used to describe the size of earthquake or the seismic energy released by an earthquake. Conventional measures of magnitude are defined based on the peak amplitude observed on seismograms from a particular instrument after correcting the attenuation to a reference distance. Seismic waves radiated from an earthquake consist of a wide spectrum of frequencies, and seismic instruments provide views into different frequency windows of seismic energy. Thus the size of an earthquake can be measured using a number of scales. In the central and eastern United States, the  $m_{Lg}$  is the widely used earthquake size measure in earthquake catalogs and therefore, we will use  $m_{Lg}$  as our magnitude in this study. However,  $m_{Lg}$  is also denoted as  $m_{bLg}$ , or  $m_{b,Lg}$ , or  $m_b(Lg)$  depending on the period used to determine the earthquake magnitude. Street (1976) and Street and Turcotte (1977) restricted the period to one second to measure  $m_{bLg}$ . But Boore and Atkinson (1987, 1988) relaxed the restriction of period to include amplitude at any period from 0 to 10 seconds. In this study, we use  $m_{Lg}$  as the magnitude measure which corresponds to the magnitude determined from amplitude of relaxed period restriction.

To convert the magnitude  $m_{Lg}$  to the seismic moment, we can first convert the  $m_{Lg}$  to the moment magnitude, then obtain the seismic moment through Equation (2.2); or directly calculate the seismic moment from  $m_{Lg}$ . There are several relationships available for eastern North America (ENA). Nuttli (1983) developed a relationship for mid-plate earthquakes

$$\log(M_0) = \begin{cases} 13.2 + 2.0 m_{Lg} & m_{Lg} \geq 4.5 \\ 17.7 + 1.0 m_{Lg} & m_{Lg} < 4.5 \end{cases} \quad (2.4)$$

Boore and Atkinson (1987) developed a moment magnitude and  $m_{Lg}$  relation based on the observation data of eastern North America earthquakes

$$M = 2.715 - 0.277 m_{Lg} + 0.127 m_{Lg}^2 \quad (2.5)$$

Somerville et al. (1988) also developed a relation between  $m_{Lg}$  and seismic moment

$$M_0 = 1.695 m_{Lg} + 14.576 \quad (2.6)$$

Johnston (1996a) derived a new seismic moment and magnitude relationship based on the data of stable continental region earthquakes

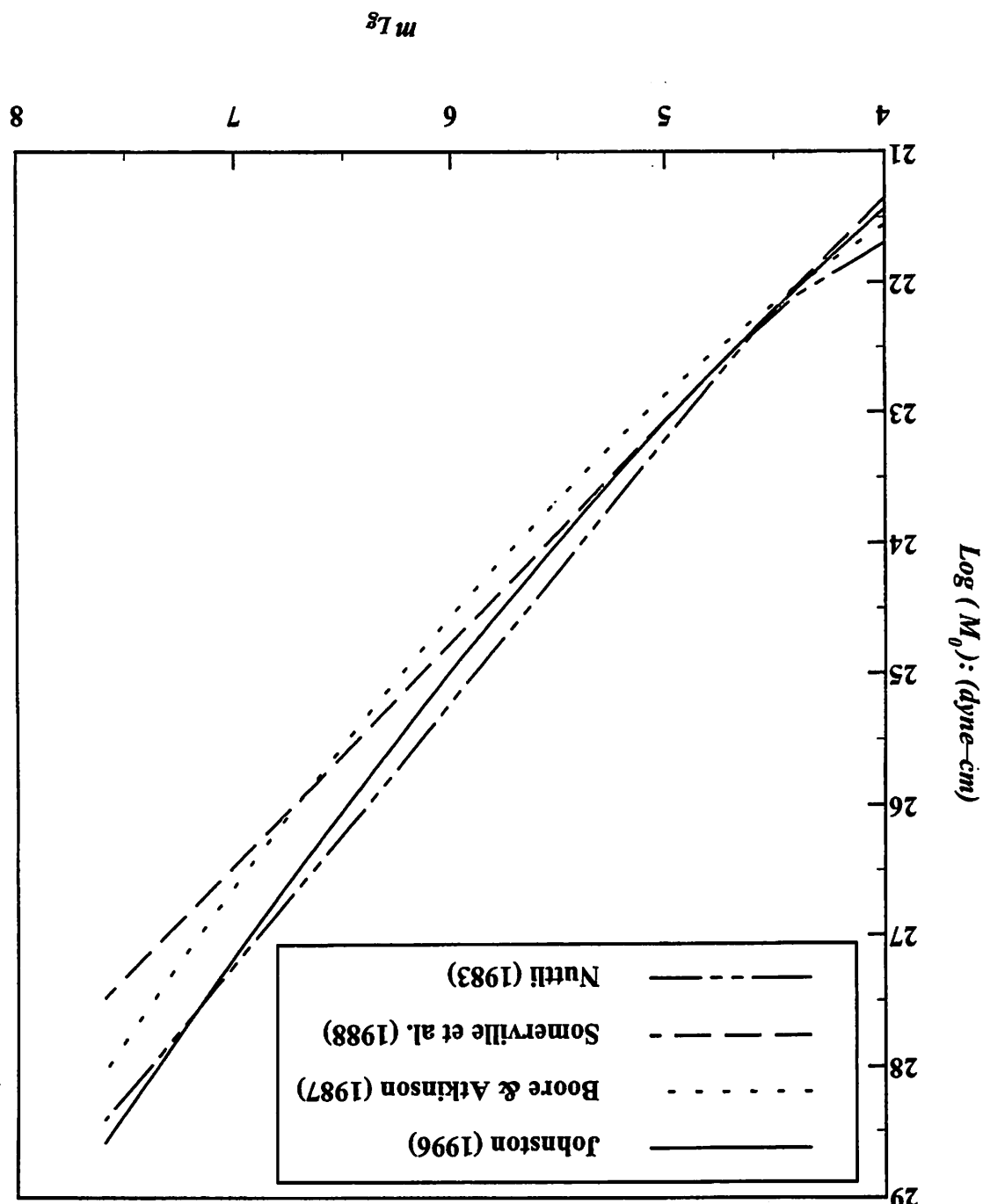
$$\log(M_0) = 17.76 + 0.360 m_{Lg} + 0.140 (m_{Lg})^2 \quad (2.7)$$

Figure 2.2 compares the above four relations of seismic moment and  $m_{Lg}$ . From Figure 2.2, it is clear that the formulas agree better for moderate magnitude than for high magnitude because there are less available data for large earthquakes. In this study, we used Johnston's (1996) relation to calculate the seismic moment from  $Lg$  wave magnitude  $m_{Lg}$ .

### 2.3.2 Focal Depth

Ground motion near the seismic source is sensitive to the source depth. Thus, for our study, it is important to determine a proper focal depth because much of West Tennessee is located within the NMSZ. The distribution of focal depth is shown in Figure 2.3 for the eastern North American earthquakes. Wheeler and Johnston (1993) characterized the focal

Figure 2.2. Comparison of the Seismic Moment and  $m_{Lg}$  Relationships  
for a Stable Continental Region.



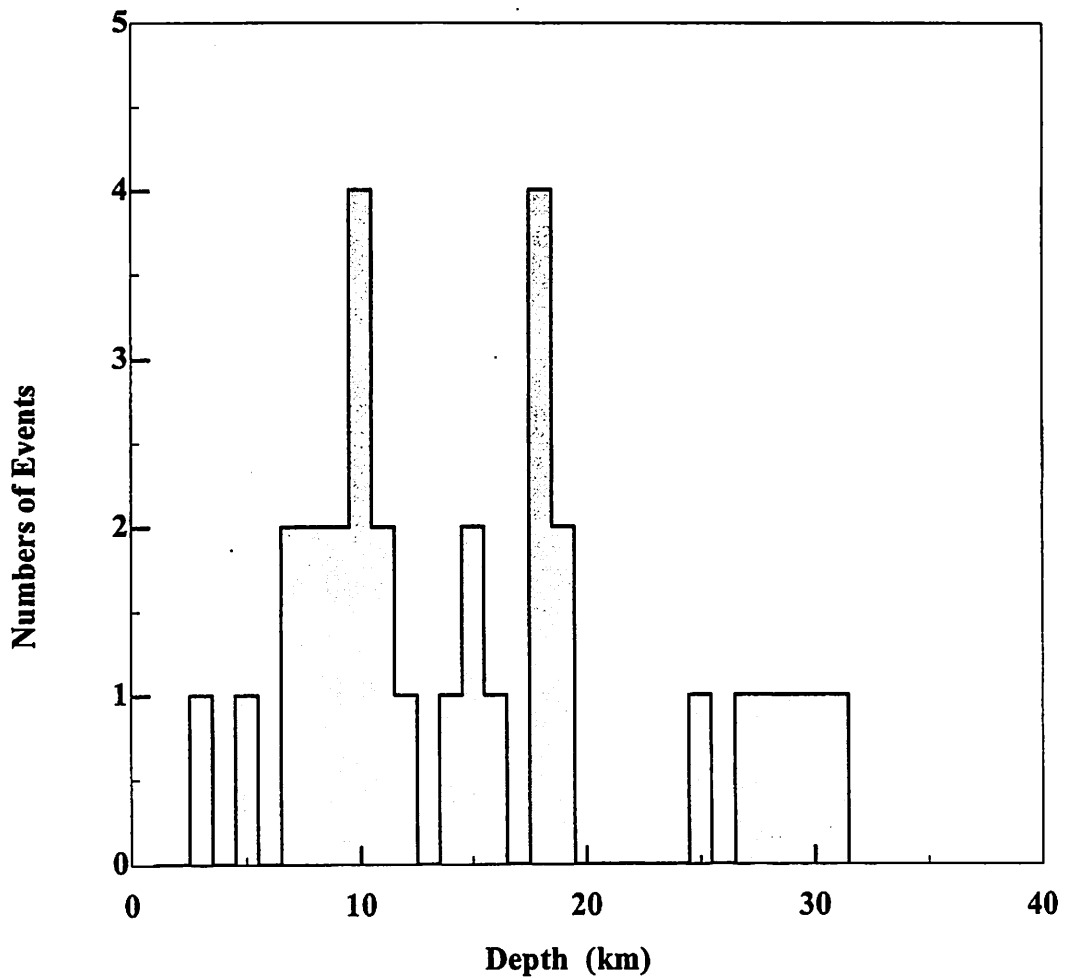


*Figure 2.3. Distribution of Focal Depth of Eastern North America Earthquakes (EPRI, 1993).*

depth of earthquakes in eastern North America as ranging from 3 to 32 km. In the NMSZ, earthquake depths are concentrated at about 7 km with a range of 5 to 12 km. Earthquakes in Appalachia are in the depth range of 5 to 8 km. EPRI (1993) showed that focal depths of stable continental region earthquakes are also concentrated at 0 to 12 km. According to Nuttli (1983a), the focal depth is about 10 km for an earthquake of  $m_b = 6$ . Therefore, we used the focal depth of 10 km.

### 2.3.3 Source Spectral Shape

The seismic source spectra are the frequency domain representation of the seismic energy released by an earthquake. Thus, a different spectral shape means a different distribution of seismic energy from low to high frequency. For most engineering purposes, one is interested in the source spectra of shear waves. Consequently, the spectral shape model discussed here is for shear wave. For the central United States, there are three seismic source spectral shape models available. The most widely used model is Brune's omega square model (Brune, 1970 and 1971):

$$S(f) = \frac{(2\pi f)^2}{1 + (f/f_c)^2} \quad (2.8)$$

where  $f_c$  is the corner frequency of seismic source, given by

$$f_c = 4.9 \times 10^6 \beta (\frac{\Delta\sigma}{M_0})^{1/3} \quad (2.9)$$

and  $\Delta\sigma$  is the stress parameter or stress drop.

From Equation (2.8), it is clear that the spectrum of ground motion is constant above the corner frequency. Therefore, if we apply an artificial or natural upper cutoff frequency, we will obtain a *band-limited random process* [6] with the corner frequency as the lower cutoff frequency. That is why most researchers treat ground motion as band-limited random process in the estimation of ground motion.

For engineering applications, the spectral amplitude above the corner frequency usually controls the ground motion. This amplitude is proportional to  $\Delta\sigma^{2/3}$ . Thus, the stress drop is an important parameter for the prediction of ground motions of engineering interest.

Because real earthquakes are highly irregular in distributions of slip, stress drop, and rupture velocity — unlike the highly simplified Brune model. The Brune model was later modified to include more complicated seismic sources. In the application of ground motion estimations, one of the modifications is to consider the similarity of earthquake sources

introduced by Joyner (1984). There are two corner frequencies in Joyner's (1984) source spectral shape model:

$$s(f) = \begin{cases} (2\pi f)^2 / (1 + if/f_B)^{1/2} & f \leq f_A \\ (2\pi f)^2 (f_A/f)^{3/2} / (1 + if/f_B)^{1/2} & f \geq f_A \end{cases} \quad (2.10)$$

where for  $M_0 \geq M_{0c}$

$$\begin{aligned} f_A &= 4.9 \times 10^6 \beta \lambda^{-1/4} (\frac{\Delta\sigma}{M_0})^{1/3} \\ f_B &= 4.9 \times 10^6 \beta \lambda^{3/4} (\frac{\Delta\sigma}{M_{0c}})^{1/3} \end{aligned} \quad (2.11)$$

and for  $M_0 \leq M_{0c}$

$$\begin{aligned} f_A &= 4.9 \times 10^6 \beta \lambda^{-1/4} \Delta\sigma^{1/3} M_{0c}^{1/6} M_0^{-1/2} \\ f_B &= 4.9 \times 10^6 \beta \lambda^{3/4} (\frac{\Delta\sigma}{M_0})^{1/3} \end{aligned} \quad (2.12)$$

where  $\lambda$  is the ratio between the length and the width of the fault. The parameter  $\lambda$  is assigned to be equal 4 as a typical value by Joyner (1984). The parameter  $M_{0c}$  is the critical moment to consider the breakdown of similarity when the seismic moment exceeds critical moment  $M_{0c}$  corresponding to rupture of the entire width of the seismogenic zone.

Based on source spectra for eastern North America, Atkinson (1993) developed a spectral shape model defined as the sum of two Brune spectra

$$S(f) = \frac{1 - \varepsilon}{[1 + (f/f_A)^2]} + \frac{\varepsilon}{[1 + (f/f_B)^2]} \quad (2.13)$$

where  $\varepsilon$ ,  $f_A$ , and  $f_B$  are functions of moment magnitude, given for  $4 \leq M \leq 7$  by

$$\log \varepsilon = 2.52 - 0.637 M \quad (2.14)$$

$$\log f_A = 2.41 - 0.533 M \quad (2.15)$$

$$\log f_B = 1.43 - 0.188 M \quad (2.16)$$

where  $M$  is the moment magnitude.

Figure 2.4 compares source spectra of the three models for moment magnitudes = 5, 6, and 7 at distance  $R = 1$  km and stress drop  $\Delta\sigma = 100$  bars for Brune and Joyner's (1984) models and critical magnitude  $M_c = 7$  for Joyner's (1984) model. We can conclude that source spectra from model by Atkinson (1993) is much higher than those by Brune and Joyner (1984) at higher frequencies but lower than those two models around corner frequencies. Around corner frequencies, Brune's model has the highest source spectral values.

There are also other source spectral models, such as the barrier model (Papageorgiou and Aki, 1983a and b). However, Brune's omega square model is still the most widely used model because of its simplicity (EPRI, 1993; and Boore et al., 1996). Moreover, this model has been successfully used to interpret strong ground motion data and  $M_L$  observations in California by many researchers (McGuire and Hanks, 1980; Hanks and McGuire, 1981; Boore, 1983; McGuire et al., 1984; and Hanks and Boore, 1984). Atkinson (1984), Herrmann (1985), Silva and Green (1988), Boore and Atkinson (1987), and Toro and McGuire (1987) have used the Brune spectra to interpret accelerograms and  $m_{Lg}$  data in eastern North America. Most importantly, the Brune model is consistent with the rock site accelerograph recordings from eastern North America earthquakes. Figure 2.5 compares observed Fourier amplitude spectra in 1982 New Brunswick and 1983 Ottawa earthquakes, and predicted values with stress drop  $\Delta\sigma = 50, 100$ , and 200 bars.

To consider the uncertainty of stress drop, we prefer to use Brune or Joyner's model as the spectral shape model because these two models include the stress drop. On the other hand, because of the simplicity of Brune's omega square model, we used the Brune model as our source spectral shape model.

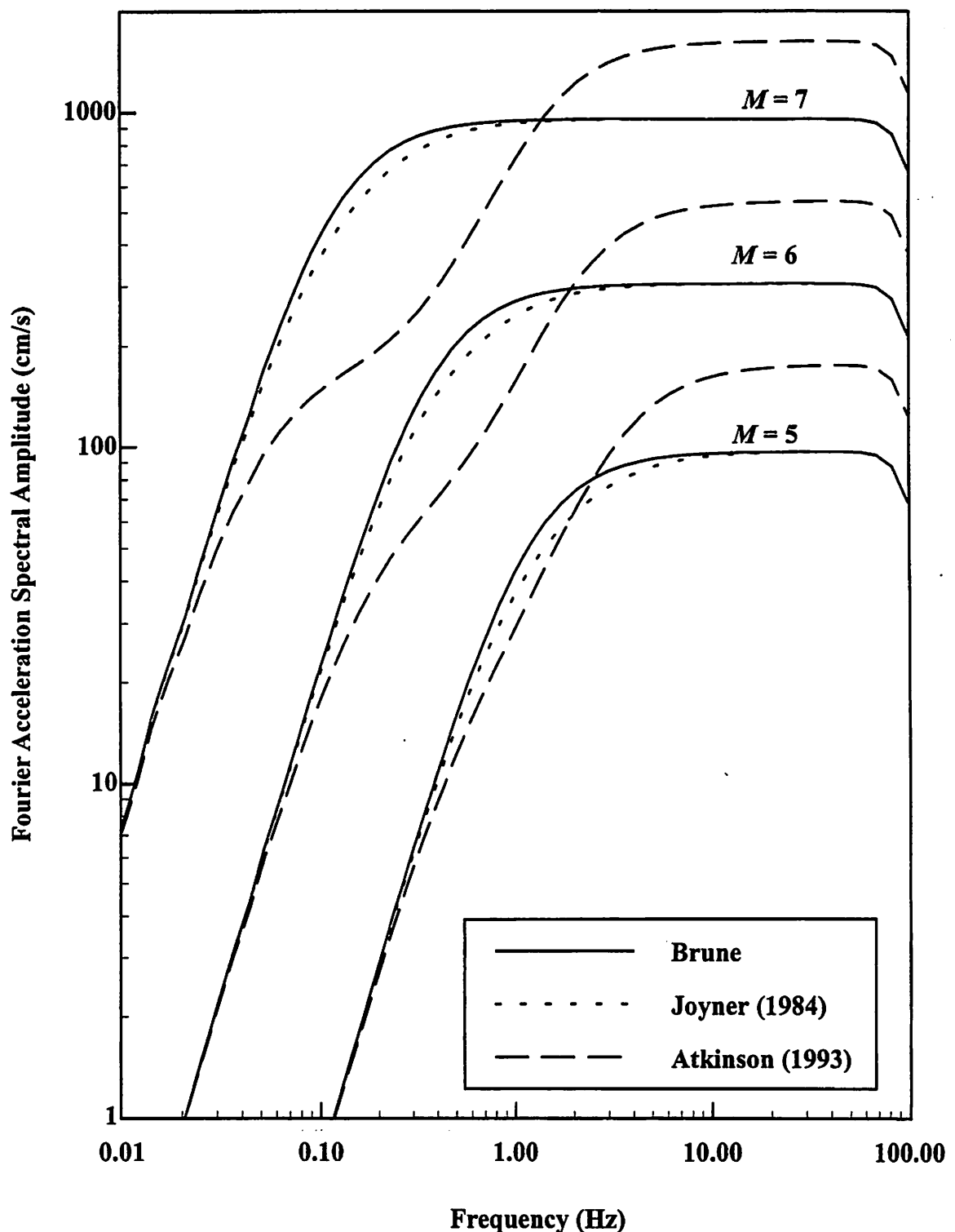
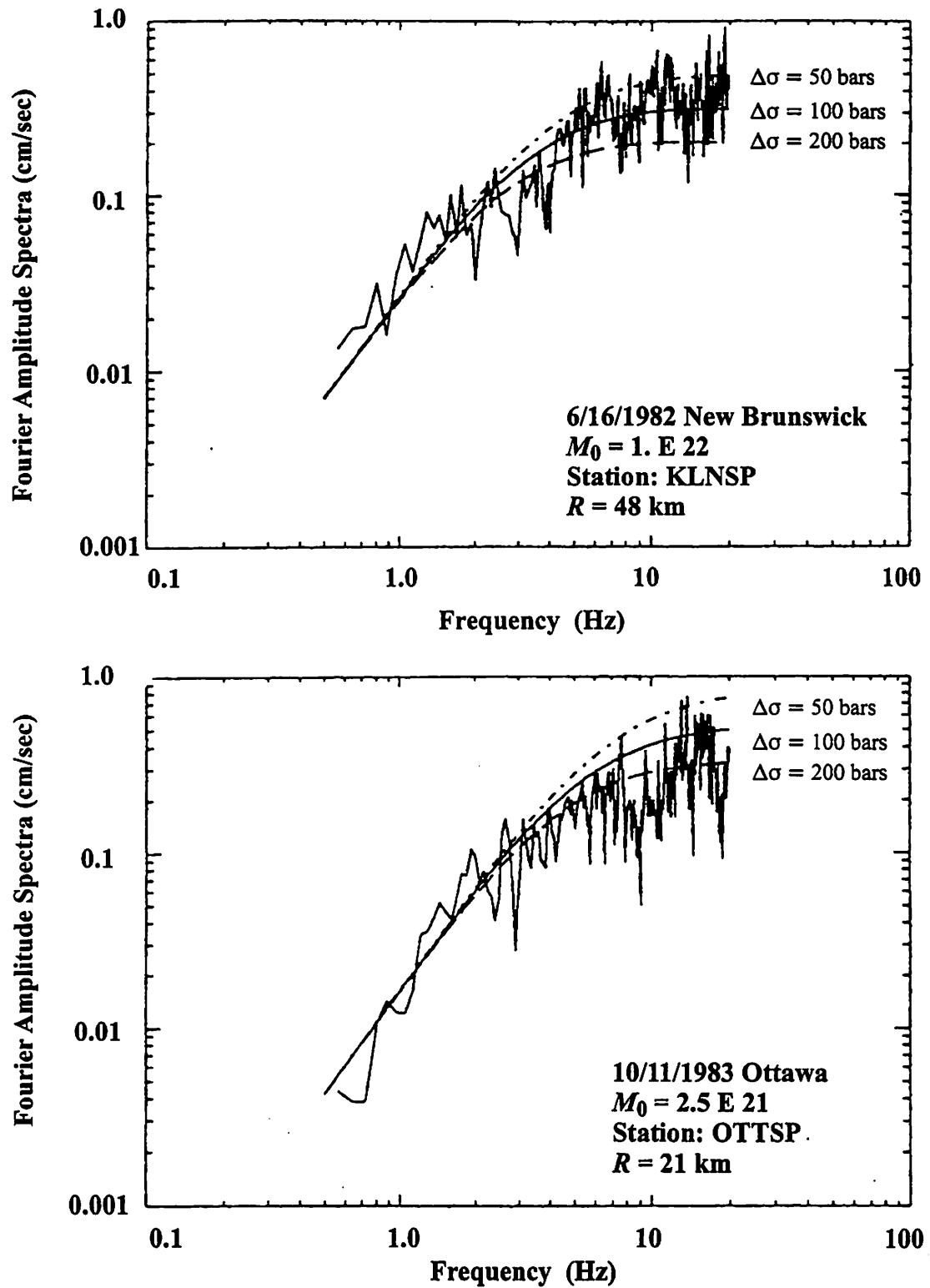


Figure 2.4. Comparison of Source Spectra of Horizontal Component for  $M = 5, 6$ , and  $7$  with  $R = 1$  km and Stress Drop = 100 bars for the Brune and Joyner Model.

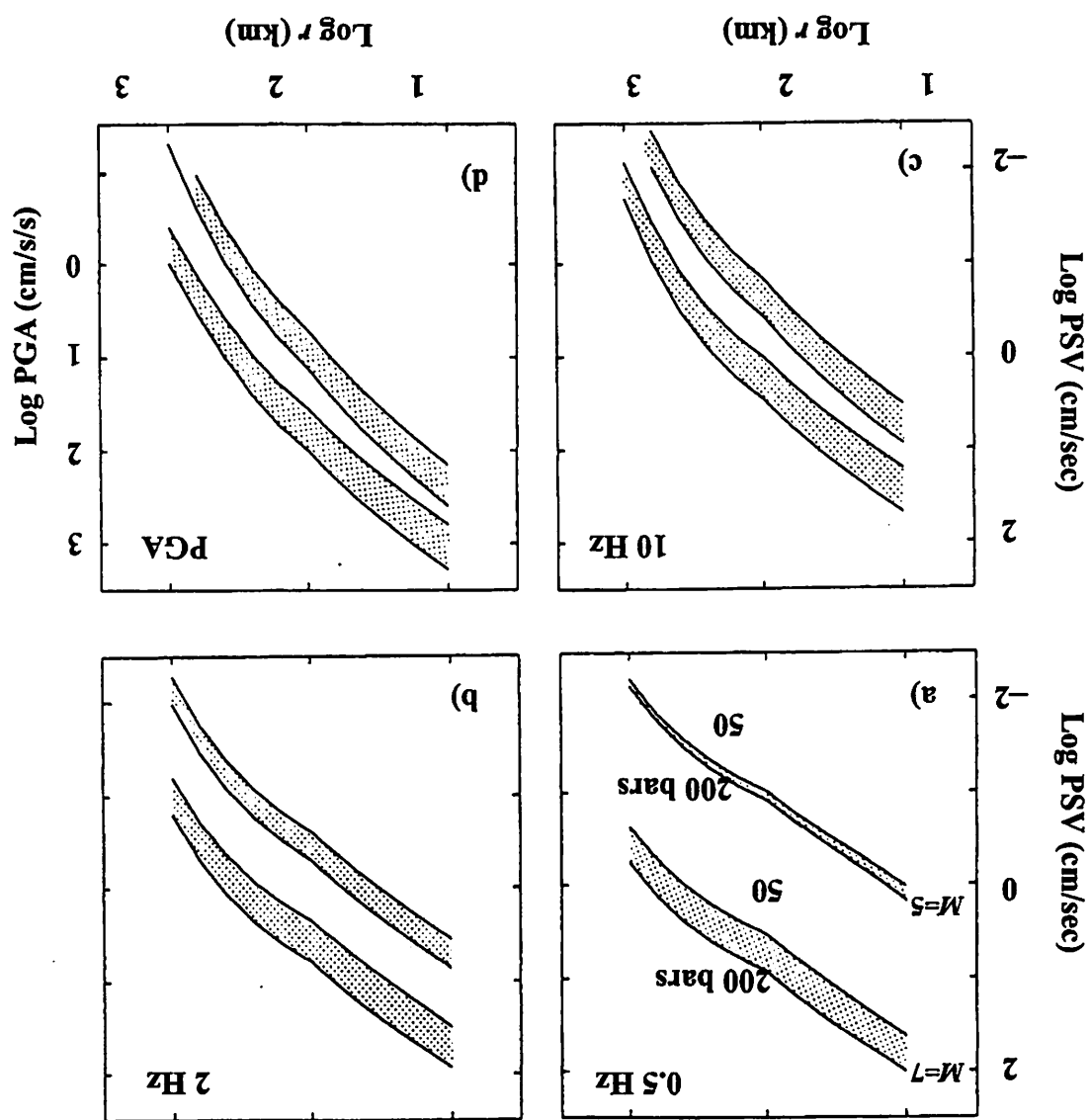


*Figure 2.5. Predicted and Observed Acceleration Spectra of two Eastern North America Earthquakes (McGuire et al., 1988).*

### 2.3.4 Stress Parameter

As mentioned earlier, in the Brune omega square model, the stress parameter determines the corner frequency of seismic source, and consequently determines the high-frequency level of acceleration spectra. The sensitivity of ground motion estimation to this parameter are shown in Figure 2.6. It is clear that stress drop has significant influence on ground motion estimation. Therefore, it is of primary importance to select a reasonable stress parameter. Unfortunately, the stress parameter is a derived rather than a measured quantity. Different researchers usually obtain different stress drops for the same region. Some researchers (Aki, 1972; Kanamori and Anderson, 1975; and Hanks, 1977) found that the stress drops were roughly independent of seismic moment and were generally in the range of 1 to 100 bars for moderate and large earthquakes. However, Nuttli (1983a and 1983b) found that stress drops increase as  $M_0^{1/4}$ . Johnston (1994) studied 83 stable continental region earthquakes. He found the stress drop ranges from 10 to more than 1000 bars with a mean stress drop of 85 bars (Figure 2.7). From Figure 2.7, it is clear that there is no correlation between the stress drop and seismic moment for the stable continental earthquakes. Even in the same region, there is no obvious relation between stress drop and seismic moment. However, stress drop does change from region to region and there is also variation within the same region. In the central and eastern North America, Atkinson (1993) found that stress drops of earthquakes range from less than 50 to over 400 bars, with a median value at about 150 bars. EPRI (1993) used a stress drop from 20 to 600 bars with 120 bars as the median for the central and eastern United States. Boore et al. (1996) used 150 bars as the stress drop for this area in the national seismic hazard zonation. Hence, the stress drop in the central and eastern United States has a mean value of about 150 bars but there are some variabilities — a range from tens to hundreds of bars. Johnston (1995, oral communication) also suggested that stress drops from 100 to 200 bars for the central United States are reasonable. To consider uncertainties of the stress drop, we used three stress drop values — 100, 150, and 200 bars.

Figure 2.6. Ground Motion Estimated for a Range of Stress Parameters  
*(From Boore and Atkinson, 1987).*



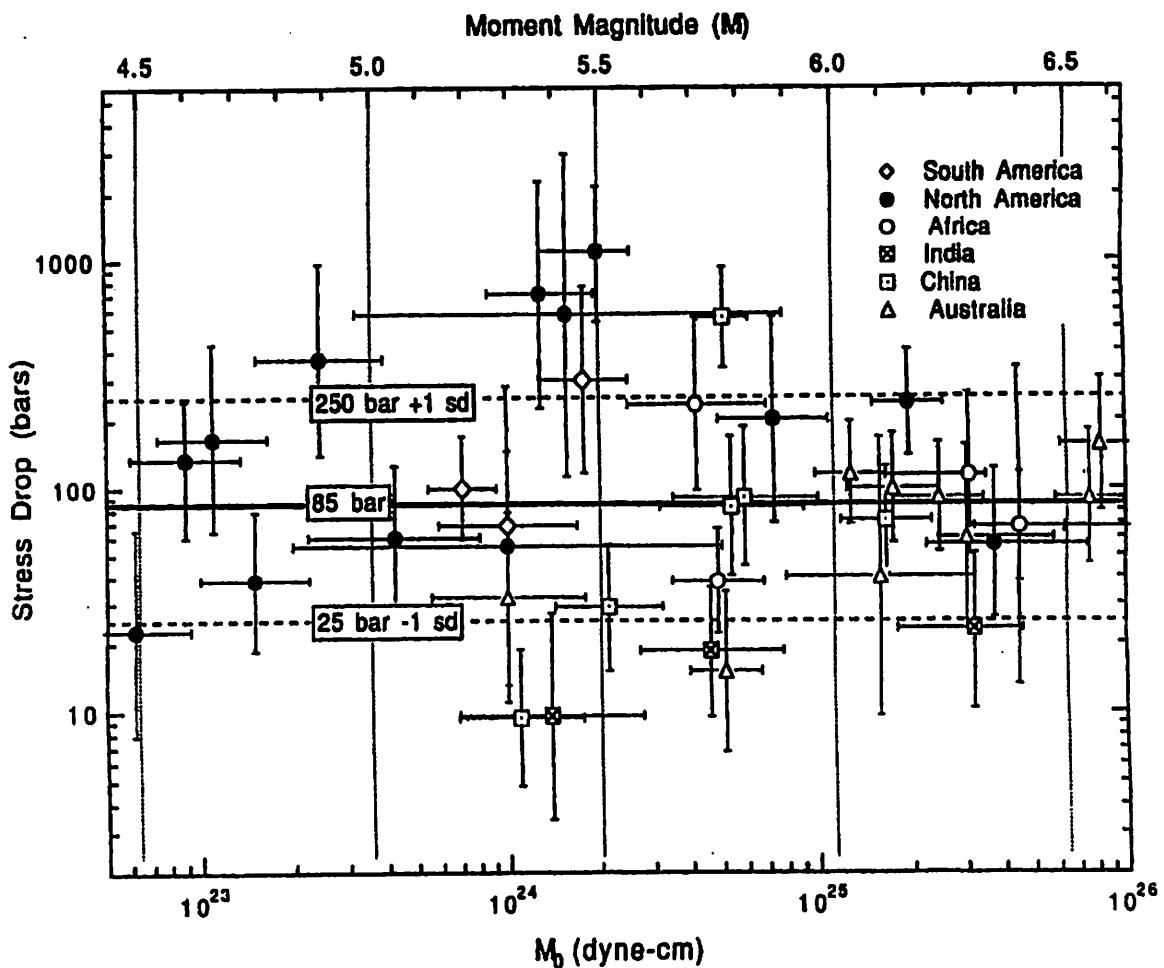


*Figure 2.7. Stress Drop Versus Seismic Moment for Stable Continental Regions (Johnston, 1994).*

## 2.4 Quantification of Propagation Path

It is well known that ground motion diminishes in amplitude with the distance from the seismic source. The attenuation of ground motion includes influences of large scale crustal velocity structure of earth, anelastic absorption of seismic energy, and scattering of seismic

waves. In Equation (2.1), the path effect is divided into two parts — geometric spreading and anelastic attenuation. The geometric spreading considers seismic waves propagating in a homogeneous whole space. The energy of a seismic wave decreases as  $R^{-1}$  while the anelastic attenuation considers the absorption, scattering, and any other features that cause the ground motion to decrease differently from the geometrical spreading.

Generally, geometric spreading is independent from the frequency of strong ground motion; therefore, it reduces the entire spectrum. On the other hand, the anelastic attenuation of the high frequency spectrum is faster than that of the low frequency spectrum, so the content of ground motion at near seismic source site is usually different from that of far field site.

#### 2.4.1 Geometrical Spreading

From the point of view of seismic waves, at short distances, shear body waves dominate the earthquake ground motion signal and carry most of the energy from the earthquake source, whereas, at large distances,  $Lg$  waves carry most of the energy. According to Herrmann and Kijko (1983), the distance in which the dominant ground motion wave shifts from shear body wave to  $Lg$  wave, is about two crustal thickness, that is approximately 70 to 100 km. At the same time, the earth is inhomogeneous. Seismic waves received at a site are the result of multiple wave arrivals, even if the distance is within 100 km. The ground motion amplitude is first controlled by upgoing direct S-waves, then by diving direct S-waves, then by post-critical reflections from mid-crustal or Moho discontinuities as the distance increases, and finally by  $Lg$  waves at a distance of about two crustal thicknesses of the study region. As a consequence, the theoretical geometric-decay curve for a given earthquake is not a smooth function of distance. The shape of this curve depends on crustal structure, source depth and mechanism, and site azimuth. Although  $R^{-1}$  was early used as the geometrical spreading in the estimation of ground motion (such as Hanks and McGuire,

1981), at a certain distance, the geometrical decay deviates from  $R^{-1}$ . Therefore, most researchers used different geometric spreading for short distance and large distance.

Herrmann (1985) took  $R = 100$  km as the turning point distance to revise the geometrical spreading to include an  $R^{-1}$  for distances less than 100 km and  $0.1R^{-1/2}$  for distances greater than 100 km. Figure 2.8 shows the average and standard deviation of

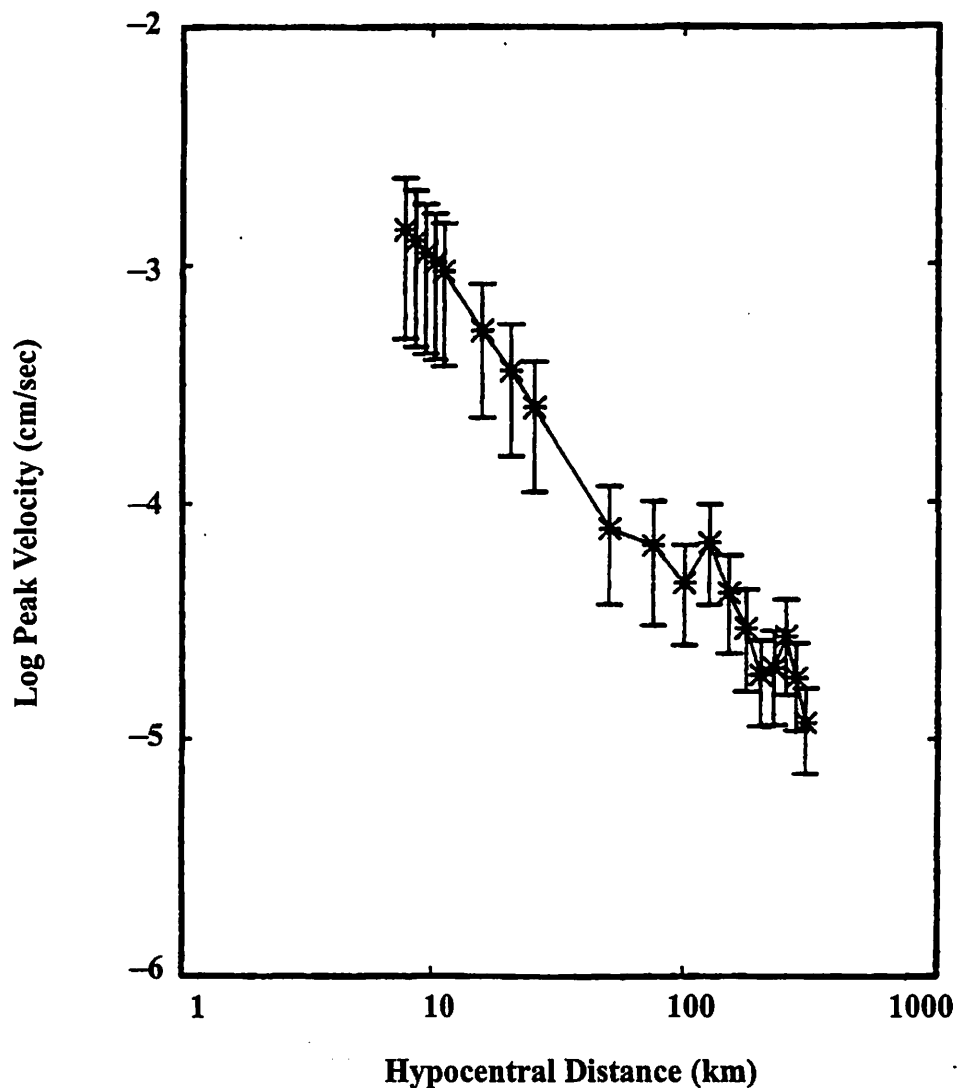


Figure 2.8. Average Peak Tangential Velocity as a Function of Hypocentral Distance for the Central United States Crustal Model of Herrmann (Revised from McGuire et al., 1988).

geometrical spreading calculated from 4,536 focal mechanisms. From this figure, we can conclude that if we consider all possible source depths and mechanisms, all possible site azimuths, variations in crustal structure, relative amplitudes, and distance ranges, the resulting average behavior is reasonably close to  $1/R$  in the range of about 10 to 100 km. Barker et al. (1988) also obtained the same average geometric spreading for horizontal spectral velocity at 5 Hz (Figure 2.9).

Atkinson and Mereu (1992) studied 1500 seismograms from 100 earthquakes with a magnitude range from  $m_N$  (Atkinson and Boore, 1987) 3 to 6.5. They concluded that

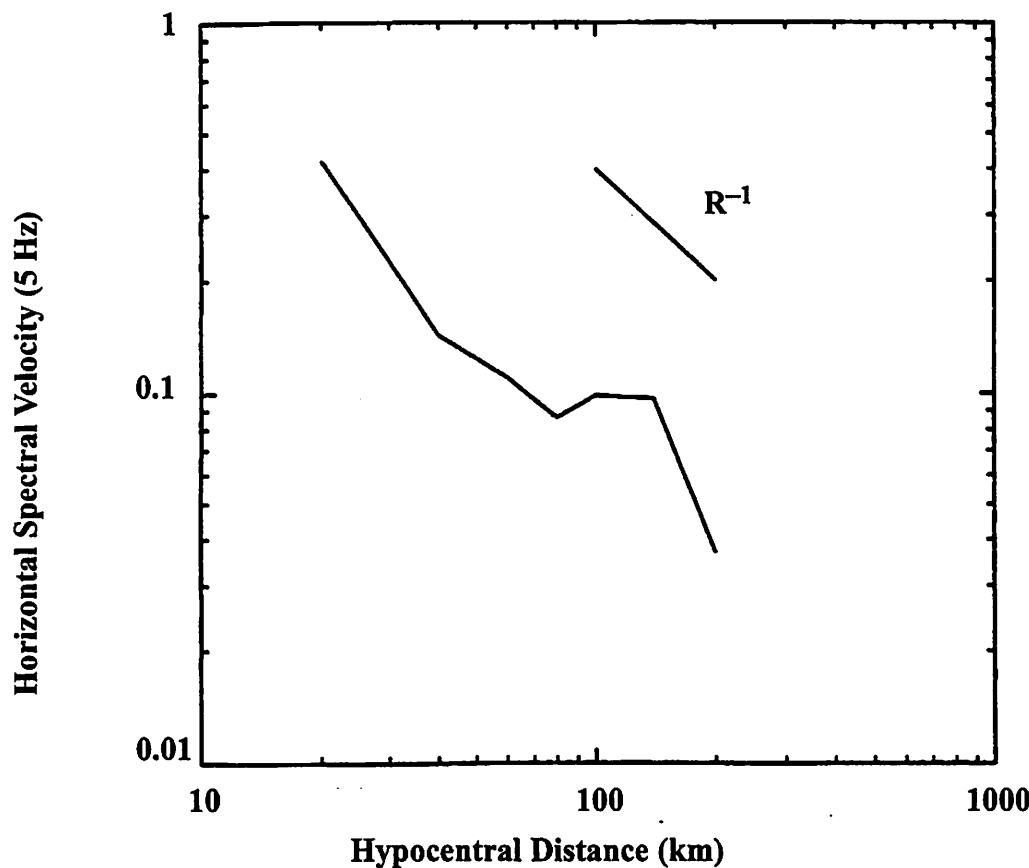


Figure 2.9. Average Geometric Spreading Obtained from the Results of Horizontal Spectral Velocity at 5 Hz. (Barker et al., 1988).

geometrical spreading is approximately independent of frequency and the best fit with observed data is given by  $R^{-1.1}$  for distances from 10 to 70 km. There is no geometrical decay from distances 70 to 130 km. The geometrical spreading can be evaluated by  $R^{-0.5}$  for distance greater than 130 km. Atkinson and Boore (1995) revised Atkinson and Mereu (1992)'s geometrical spreading as following:

$$G(R) = \begin{cases} \frac{1}{R} & 1 < R \leq 70 \text{ km} \\ \frac{1}{70} & 70 < R \leq 130 \text{ km} \\ \frac{1}{70} \sqrt{\frac{130}{R}} & R \geq 130 \text{ km} \end{cases} \quad (2.17)$$

Figure 2.10 shows geometrical spreading of Equation (2.17). Boore et al. (1996) used this relation as the geometrical attenuation of seismic waves in national seismic hazard zonations.

At distances beyond 100 km,  $Lg$  waves dominate high-frequency ground motion. Shin and Herrmann (1987) compared the simulated and the observed seismogram, and showed that the geometric spreading was well described by  $R^{-1/2}$  for distances larger than 100 km in the eastern North America. Although Atkinson (1989) suggested that there is no difference of geometric spreading at a distances less than and greater than 100 km for some earthquakes, many researchers (Herrmann, 1985; Atkinson and Boore, 1995; and Boore et al., 1996) used different geometric decay for distances less and greater than 100 km. Ou and Herrmann (1990) developed a more complicated geometrical spreading model to include the effects of direct and supercritically reflected waves in a crustal structure.

From these comparisons of geometrical spreading (Figures 2.8, 2.9, and 2.10), it is clear that for distances less than about 70 km, geometrical spreading is roughly equal to  $R^{-1}$ . From about 70 to 150 km, there is no obvious geometrical decay. For distances over 150 km, the geometrical decay is much slower than that of less than 70 km. Therefore, we used Equation (2.17) as the geometrical spreading.

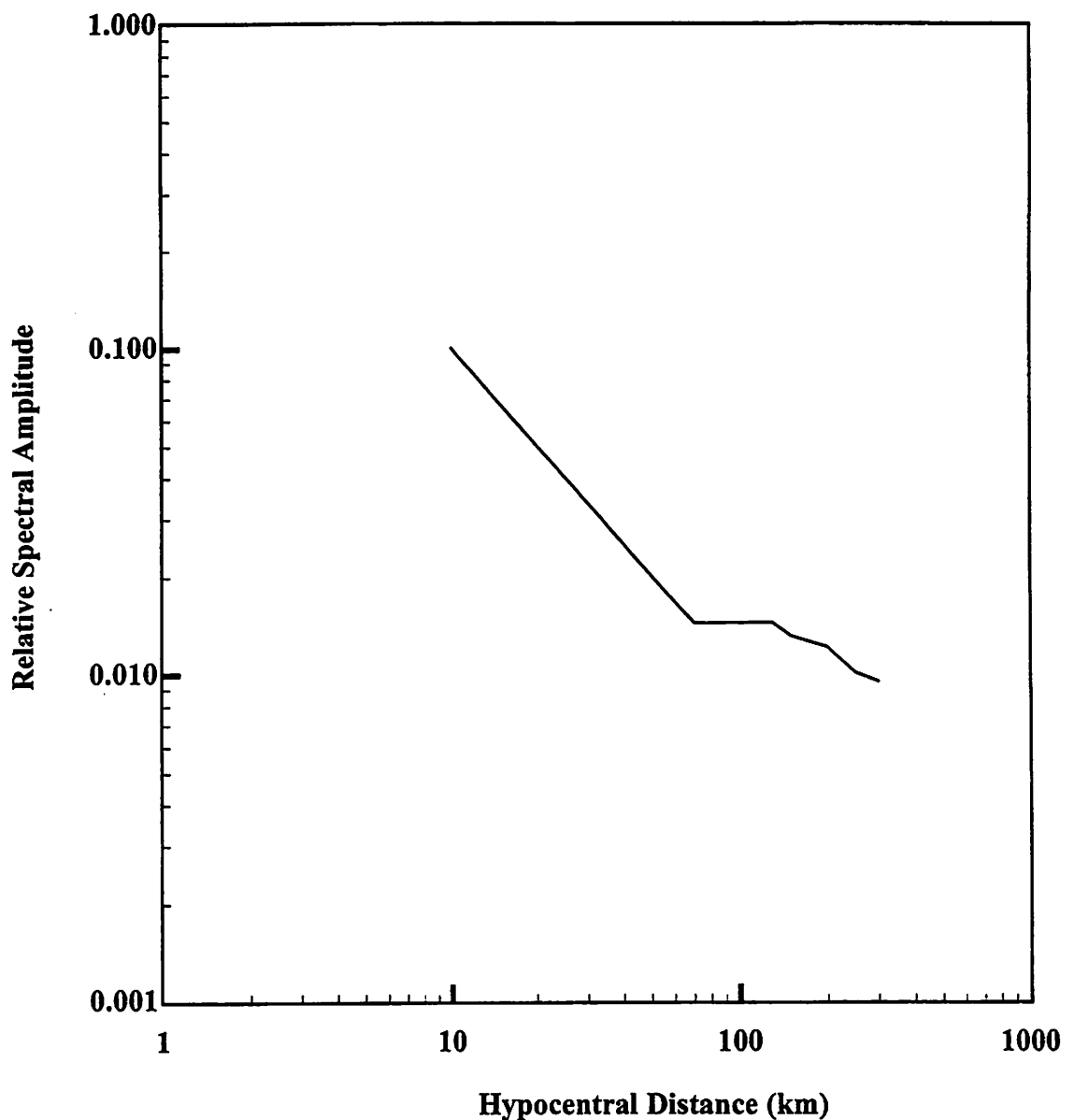


*Figure 2.10. Geometrical Spreading Used by Atkinson and Boore (1995) and Boore et al. (1996).*

#### 2.4.2 Anelastic Attenuation

The anelastic attenuation term in Equation (2.1) can be represented by

$$D(R, f) = \exp\left[-\frac{\pi f R}{Q(f) \beta}\right] \quad (2.18)$$

where  $Q(f)$  are frequency dependent quality factors. As mentioned earlier, the anelastic attenuation represents any factors causing ground motion amplitude decay other than geometrical spreading. Many factors may affect anelastic attenuation, such as the crustal structure and its properties. Crustal structures and properties vary with geological regions and ages, so the anelastic attenuation of seismic waves is region dependent. At the same time, because of the complexity of crustal properties, varieties of factors which may affect the anelastic attenuation, and the sparseness of strong ground motion recordings, it is impossible to obtain a consistent  $Q(f)$  value for a specific region. Many investigators have performed empirical studies on the effect of anelastic attenuation on ground motions for central and eastern North American.

Nuttli and Dwyer (1978) studied attenuation of high-frequency (1-10 Hz) seismic waves in the central Mississippi valley using vertical components of 89 microearthquakes which occurred in the NMSZ between 8/16/74 and 2/13/77. They found that the  $Q(f)$  factor of  $L_g$  waves seems constantly to be 1500, at frequencies of 1 to 10 Hz. Compared with  $Q(f)$  factors in tectonic regions such as California or Japan, which usually have  $Q(f)$  factors of 200-250, the high  $Q(f)$  factor of 1500 indicates that high frequency  $L_g$  waves will propagate to much greater distances in the central Mississippi valley than in tectonic regions.

Dwyer et al. (1983) studied this spatial attenuation of  $L_g$  waves in the central United States using both broadband and narrow-bandpass-filtered time-domain data obtained from events occurring in the NMSZ. Dwyer et al. (1983) used a least-square technique to determine coefficients of anelastic attenuation at various frequencies obtaining a frequency dependent  $Q(f)$  factor for the this area as

$$Q(f) = 1500 f^{0.4 \pm 0.15} \quad (2.19)$$

Equation (2.19) was also used by Johnston (1988) in his study if bedrock acceleration in the Memphis area due to large New Madrid earthquakes, and by Nuttli and Herrmann (1984)

in their study on source characteristics and strong ground motion of New Madrid earthquakes.

Dwyer et al. (1984) used 109 digital records from the central Mississippi valley seismic network to study regional  $L_g$  wave attenuation and coda  $Q(f)$  factor in the central Mississippi valley. They obtained the following equations. From coda  $Q(f)$ ,

$$Q(f) = \begin{cases} 228 f^{0.73} & \text{(for surface wave)} \\ 270 f^{0.87} & \text{(for body wave)} \end{cases} \quad (2.20)$$

and from  $L_g$  waves,

$$Q(f) = 210 f^{0.78} \quad (2.21)$$

Hasegawa (1985) studied attenuation of  $L_g$  waves in the Canadian Shield using the digital data of vertical components of  $L_g$  waves recorded by the Eastern Canada Telemetered Network (ECTN). Magnitude ( $m_{Lg}$ ) ranges from 2.8 to 5.2, epicentral distance (Pezeshk et al., 1996) from 70 to 900 km, and frequency from 0.6 to 20 Hz. For the vertical component of  $L_g$  waves traversing the Canadian Shield, he obtained

$$Q(f) = 900 f^{0.2} \quad (2.22)$$

Gupta et al. (1987 and 1988) studied band-pass-filtered  $L_g$  amplitudes from 107 eastern North America earthquakes and obtained the following relation for  $L_g$  amplitudes,

$$Q(f) = 982 f^{0.376} \quad (2.23)$$

Shin and Herrmann (1987) studied  $L_g$  attenuation using data from earthquakes in the 1982 Miramichi earthquake source zone. They found that the dependence of  $L_g$ - $Q$  with frequency can be approximately modeled by the relation

$$Q(f) = (500 f^{0.65} - 550 f^{0.65}) \quad (2.24)$$

Atkinson and Mereu (1992) studied 1500 seismograms from 100 small to moderate earthquakes; they found the  $Q(f)$  value as

$$Q(f) = 670 f^{0.33} \quad (2.25)$$

This relation was later modified by Atkinson and Boore (1995) as

$$Q(f) = 680 f^{0.36} \quad (2.26)$$

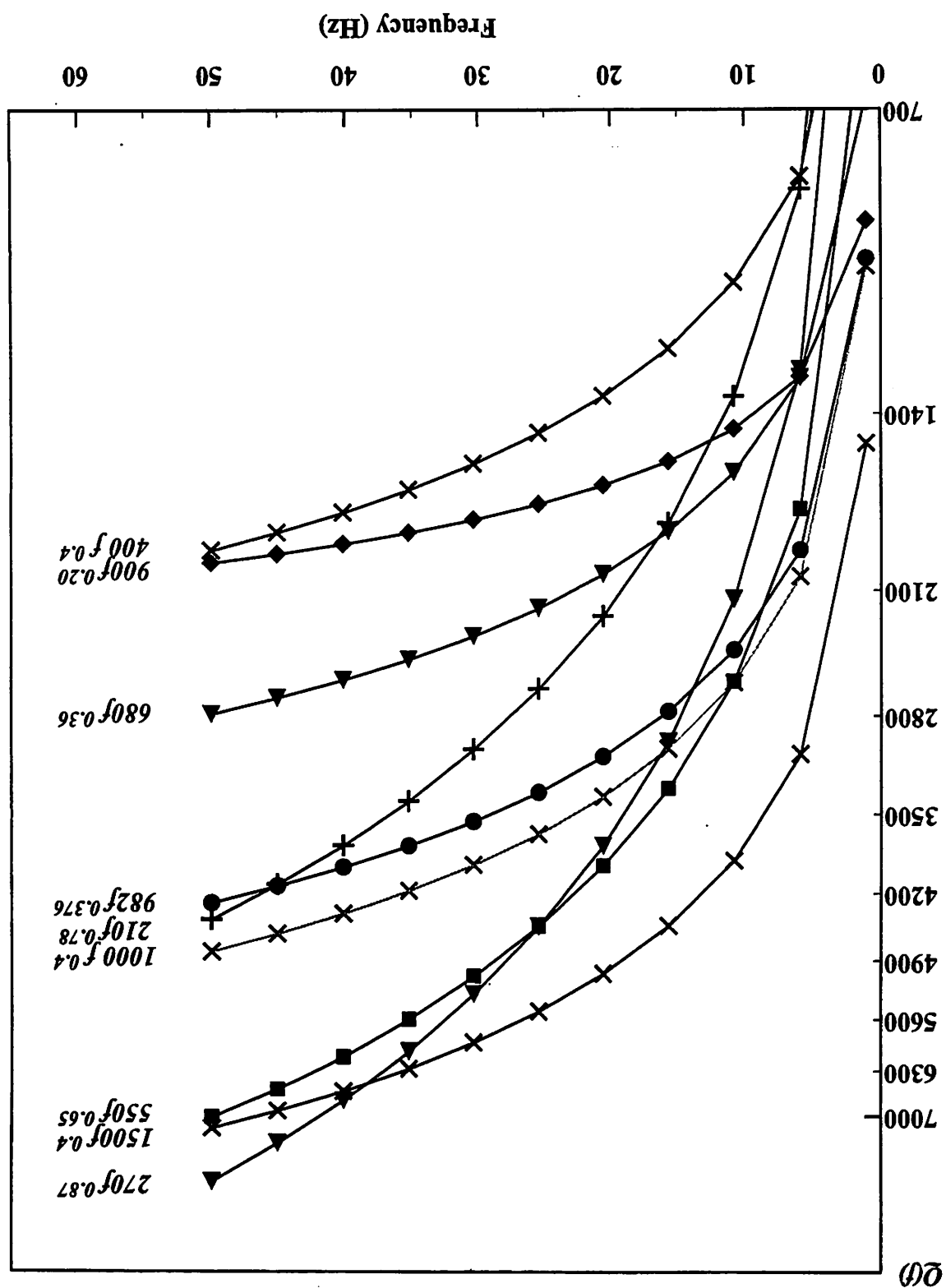
They then used this relation to predict ground motion in the ENA. Boore et al. (1996) also used this relation to determine the ground motion attenuation for central and eastern United States. EPRI (1993) used Equation (2.25) as the median of seismic wave attenuation for the central and eastern United States with the range of attenuation as following

$$Q(f) = 400 f^{0.40} \quad (2.27)$$

$$Q(f) = 1000 f^{0.40} \quad (2.28)$$

Figure 2.11 compares above  $Q(f)$  functions. From these relations, we can conclude that the variation of  $Q(f)$  value is very large. To consider these uncertainties in the estimation of quality factors, we used in this study the body wave and  $Lg$  wave attenuations of Atkinson and Boore (1995) and Dwyer et al. (1984). We use these two attenuation relations because the former is accepted as the quality factor of central and eastern United States (EPRI, 1993; and Boore et al., 1996) and the latter is based on the observed data in the NMSZ. We used Atkinson and Boore's (1995)  $Q(f)$  for distances greater than 1 km while we used the body wave relation and  $Lg$  wave relation from Dwyer et al. (1984) for distances less than and greater than 100 km, respectively.

Figure 2.11. Comparison of Quality Factor  $Q(f)$  for the Central and Eastern United States.



## 2.5 Near Site Effects

Two near site effects must be considered in the estimation of ground motions: One is the high-cut filter which represents the rapid depletion of seismic energy above a certain frequency and the other is amplification to account for the influence of rock properties beneath the site on the ground motion.

### 2.5.1 High-cut Filter

In the prediction of ground motion, Fourier amplitude spectra of acceleration are constant in theoretical source spectral models (such as Brune model). However, the Fourier acceleration spectra observed accelerograms usually fall off rapidly beyond some frequency. Hanks (1982) attributed the spectral fall-off to the near site attenuation. Papageorgiou and Aki (1983a and b) consider the fall off of acceleration spectra as the influence of seismic source. Anderson and Hough (1984) studied ground motion recordings in California and concluded the spectral fall-off is caused by the subsurface geological structure near the site.

The high-cut filter in Equation (2.1) may be written as

$$P(f, f_m) = [1 + (f/f_m)^{2n}]^{-1/2} \exp(-\kappa\pi f) \quad (2.29)$$

where  $f_m$  is the high-cut frequency or the high frequency limit in the ground motion (Hanks, 1982),  $n$  is the order of *Butterworth filter* [7] (usually  $n = 4$ ), and  $\kappa$  is the site and distance dependent factor.

The first and second terms in Equation (2.29) were introduced by Boore (1983) and Anderson and Hough (1984), respectively. In the application, most researchers use only the second term in Equation (2.29). Figure 2.12 compares observed Fourier amplitude spectra of acceleration and predicted values with different high-cut filters. We can see from Figure 2.12 that a value of 0.004 for  $\kappa$  results in better fit to the observed data compared to other values of  $\kappa$ .

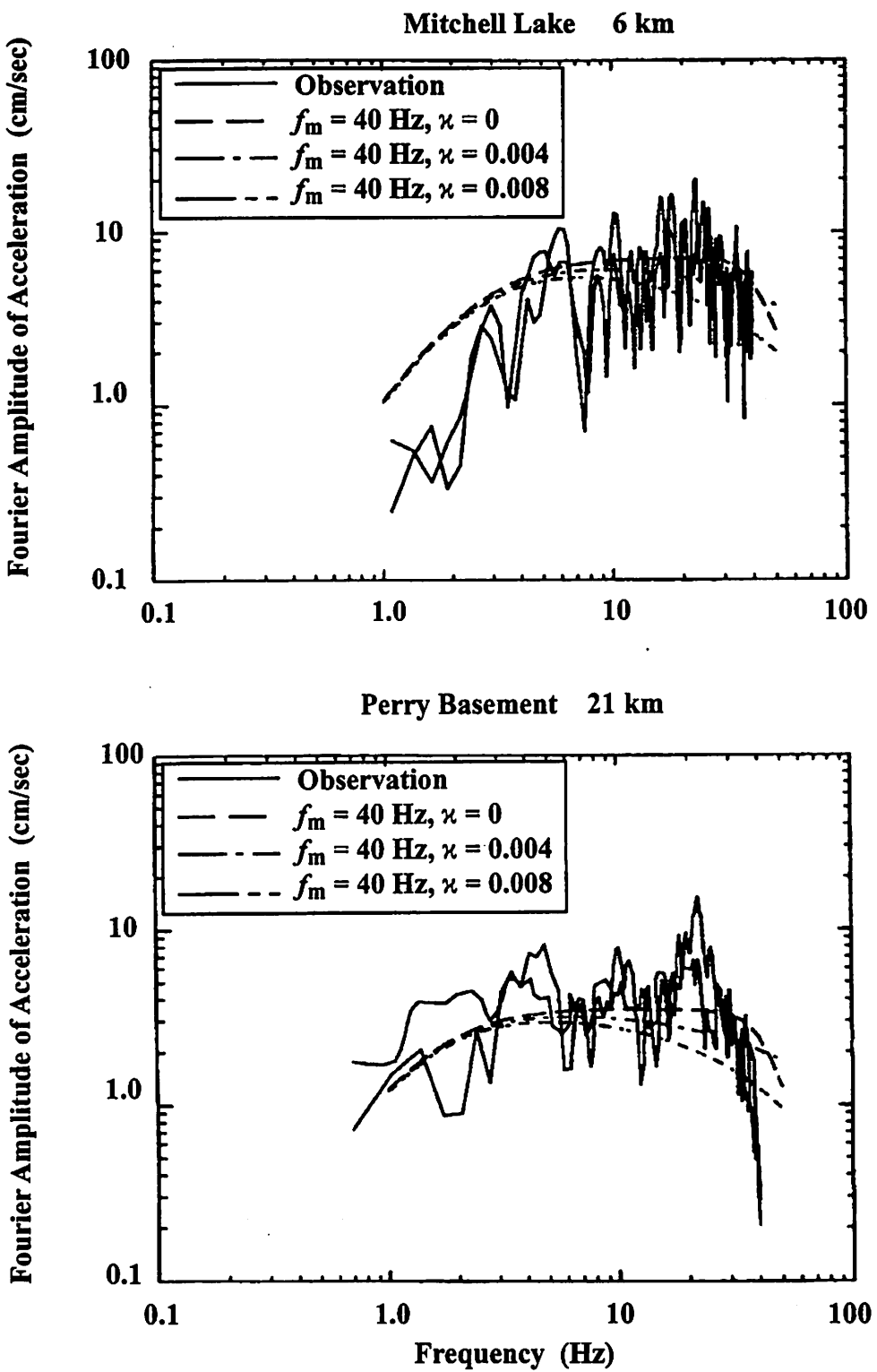


*Figure 2.12. Comparison of Observed and Brune Fourier Amplitude Spectra Using Different High-Cut Filters (Revised from McGuire et al., 1988).*

Theoretically,  $\alpha$  is a site and distance dependent parameter that accounts for the effect of attenuation on seismic waves as they propagate through the crust from source to receiver (or site). However, most researchers use distance independent and site dependent  $\alpha$ . Hough et al. (1988) attributed the  $\alpha$  value to attenuation in the very shallow crust directly beneath the site. Silva and Darragh (1993) suggested that the influence of crust on  $\alpha$  may extend to as deep as 1 to 2 km. In the western North America (WNA), an average value of  $\alpha$  is between 0.02 and 0.06 sec. However, in the ENA, high frequency contents of the ground motion are much higher than that in the WNA. Figure 2.13 compares the average spectral shape of the 1988 Nahanni earthquake ( $M = 6.8$ ) at hard rock with the average spectral shape of both the 1971 San Fernando earthquake ( $M = 6.6$ ) and the 1979 Imperial Valley earthquake ( $M = 6.4$ ). It implies that the  $\alpha$  value in the ENA be less than that in the WNA.

Silva and Darragh (1993) suggested  $\alpha = 0.006$  second for hard rock in the ENA. EPRI (1993) adopted  $\alpha = 0.006$  second as the median value of  $\alpha$ . Boore et al. (1996) used the same value for the  $\alpha$  in hard rock. Figures 2.14 to 2.16 compare observed and predicted hard rock acceleration spectral shapes with  $\alpha = 0.006$  second for some ENA earthquakes. It is clear that the value of  $\alpha = 0.006$  second is reasonable for hard rock in ENA. Moreover, from Figures 2.14 to 2.16, the high-cut frequency is over 50 Hz corresponding to  $\alpha = 0.006$  second which is higher than that used by previous researchers (Boore and Atkinson, 1987; McGuire et al., 1988; and Toro et al., 1992).

### 2.5.2 Near Site Amplification

Near site or surface amplification factors account for the increase in amplitude as seismic waves travel through lower-velocity crustal layers near the ground surface (Boore, 1986). To calculate amplification factors, Joyner et al. (1981) introduced a quarter-wavelength approximation method. At a specific frequency, the amplification is given by the square root of the ratio between the seismic impedance (shear wave velocity

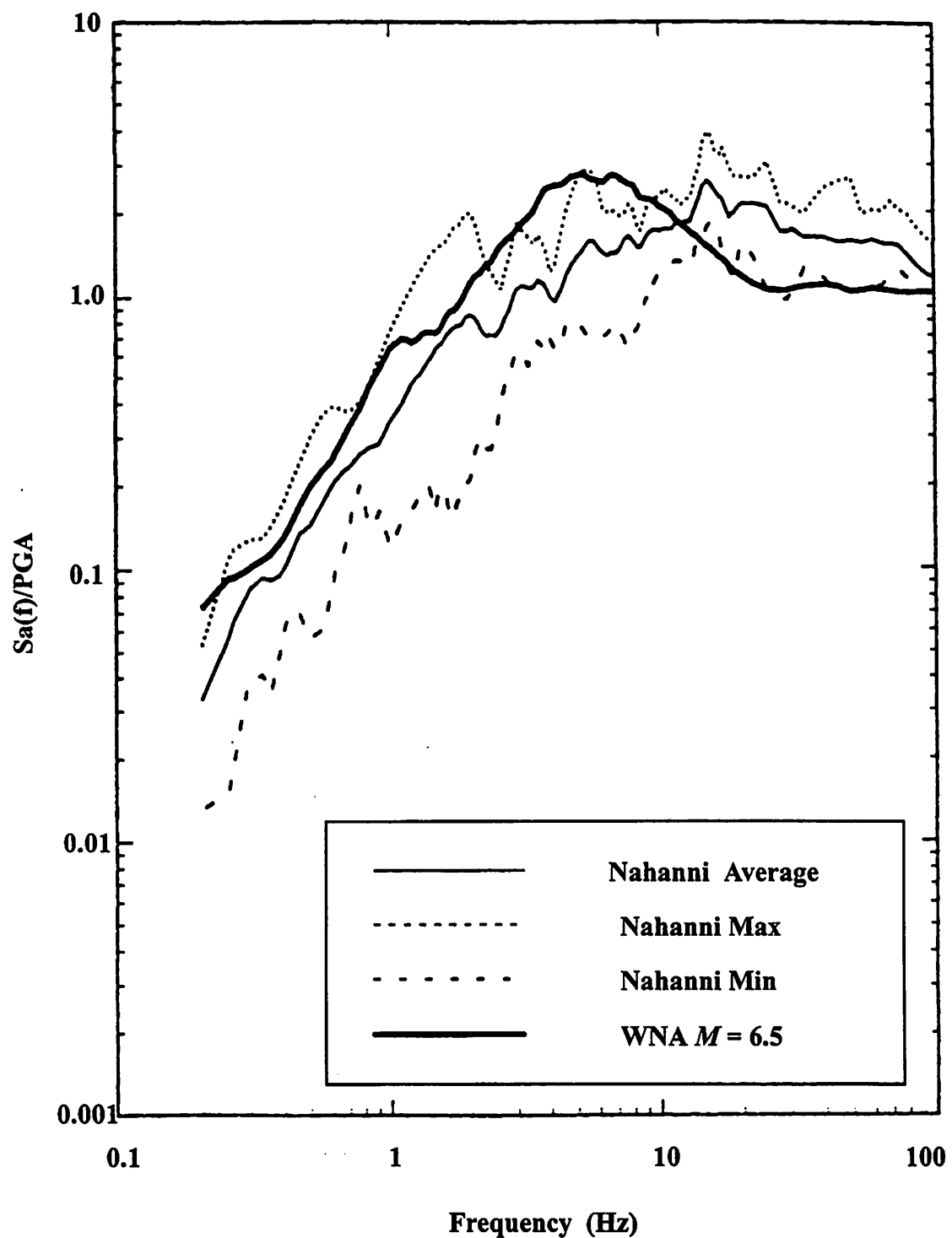


Figure 2.13. Comparison of an Average Spectral Shape at the Hard Rock Site (Nahanni).

Figure 2.14. Comparison of Recorded and Predicted Response Spectra  
Shapes for ENA Hard Rock Sites for  $M = 4.0$  to  $4.8$ .

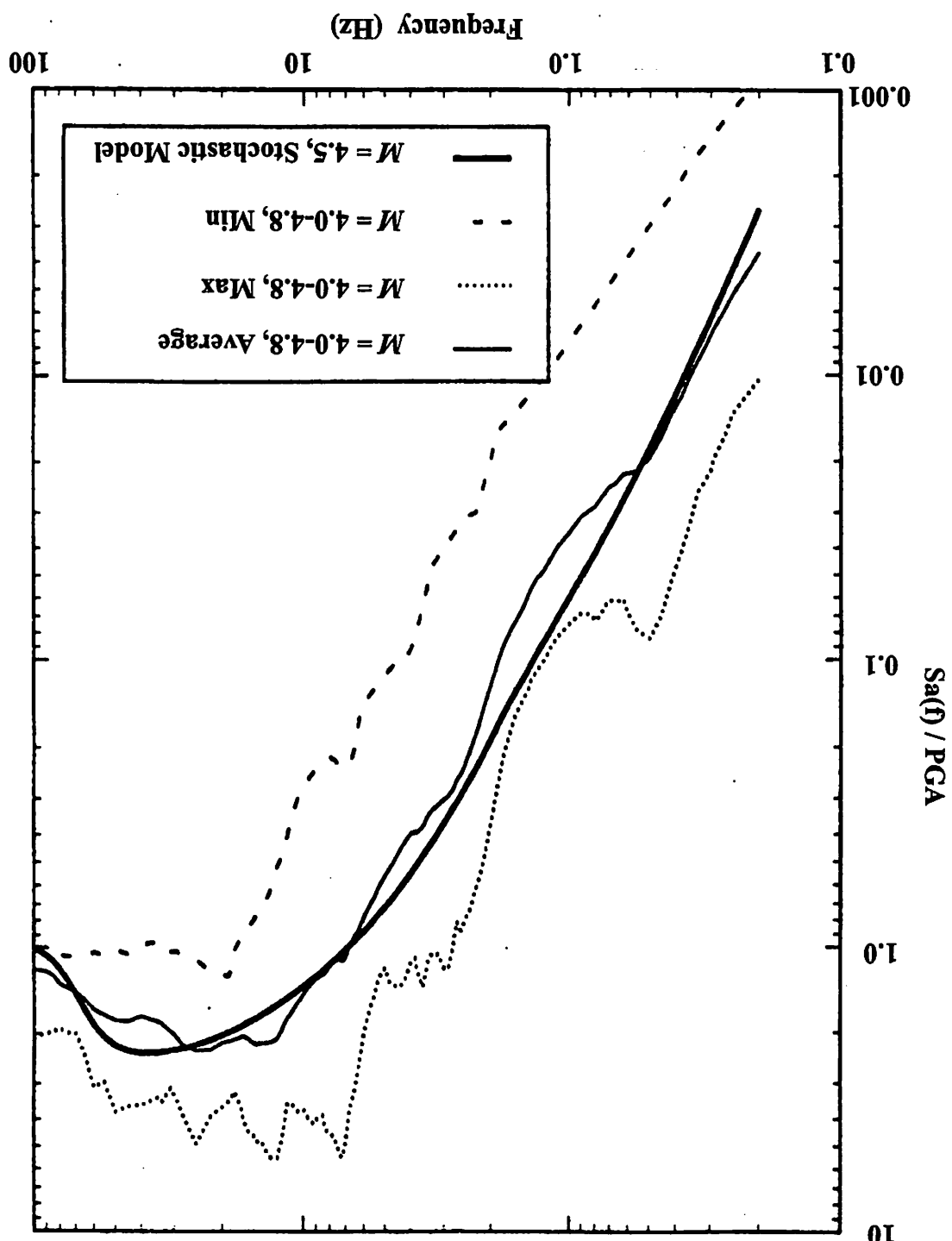
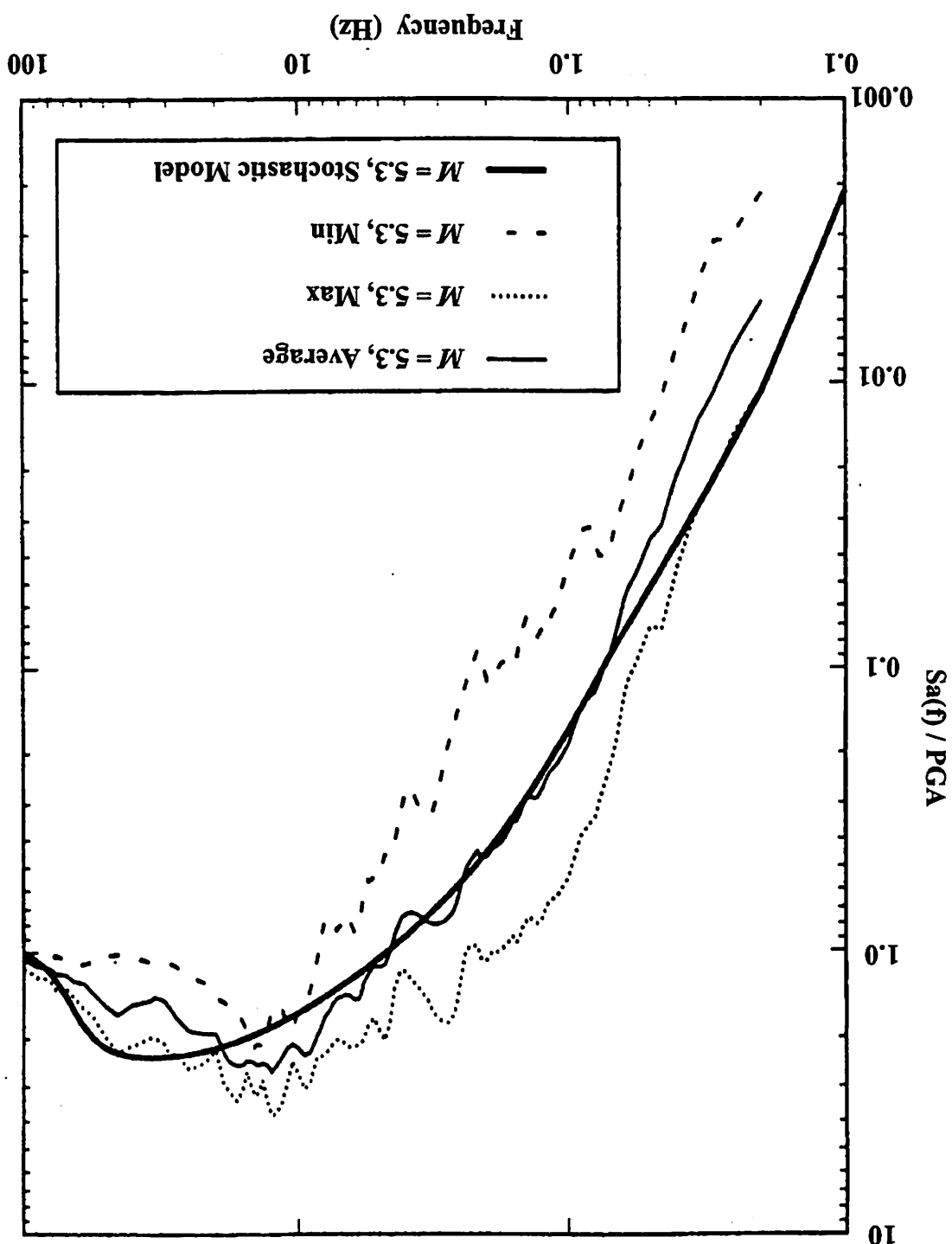
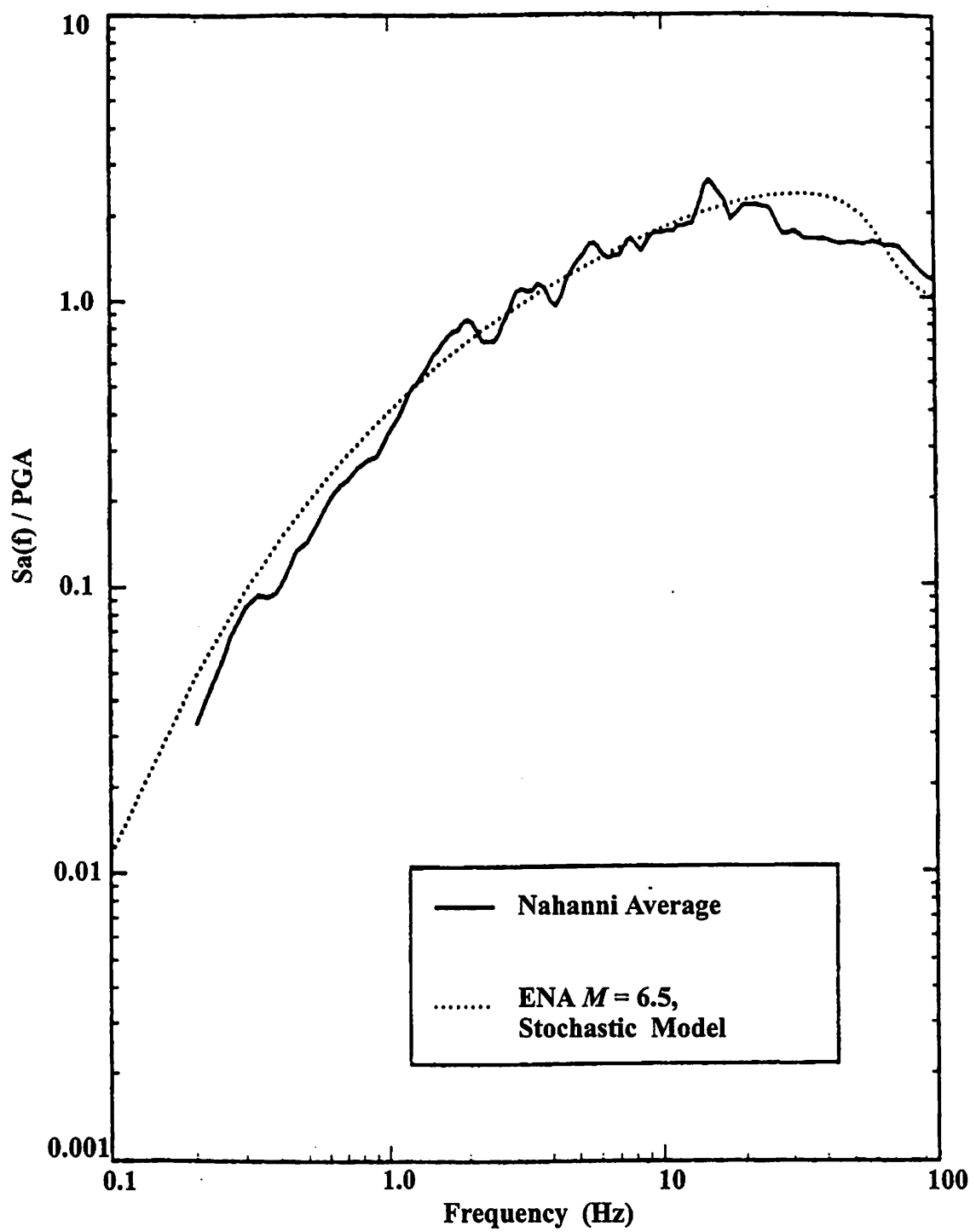


Figure 2.15. Comparison of Recorded and Predicted Response Spectral Shapes for ENA Hard Rock Sites for  $M = 5.4 - 5.7$ .





*Figure 2.16. Comparison of Recorded and Predicted Response Spectral Shapes for ENA Hard Rock Sites for  $M = 6.5$ .*

times density) at focal depth and the seismic impedance averaged over a depth from surface to a quarter wavelength

$$Am(f) = \sqrt{\frac{\rho_s \beta_s}{\bar{\rho} \bar{\beta}}} \quad (2.30)$$

where  $\rho_s$  and  $\beta_s$  are the density and shear wave velocity at seismic source;  $\bar{\rho}$  and  $\bar{\beta}$  are the average density and shear wave velocity of crust in the upper quarter wavelength.

It is clear that amplification factors depend on properties of crust. To estimate amplification factors, we have to understand crustal structures, shear wave velocities or P-wave (Pezeshk et al., 1996) velocities, and densities of crustal layers. Figure 2.17 shows

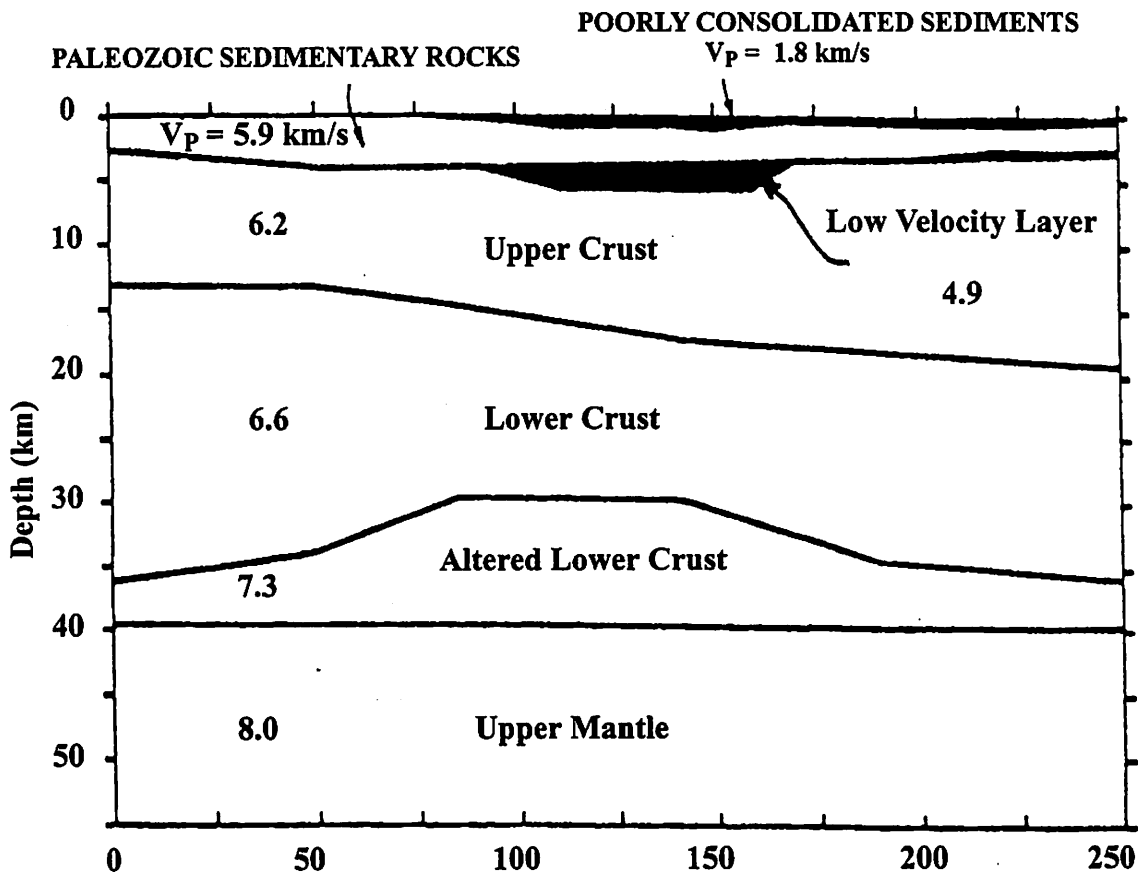


Figure 2.17. Crustal Model for the New Madrid Area  
(Mooney and Andrews, 1984).

the crustal model in the NMSZ. From Figure 2.17, we observe that crustal structures are different from other areas because of the Mississippi Embayment. At the same time, crustal layers are not horizontally distributed. Therefore, we can obtain different velocity structures for this area if we use earthquake recording data from different locations.

For the study area, there are several crustal velocity structures available. Nuttli et al. (1969) developed a velocity structure for the New Madrid area based on earthquake observation in the central Mississippi valley. Andrews et al. (1985) and Chiu et al. (1992) also developed velocity structures for the New Madrid area. Saikia et al. (1992) derived a velocity structure through modeling body and surface wave from earthquake and explosion near Dyersburg, Tennessee. Table 2.1 lists above crustal models for the New Madrid region and Figure 2.18 compares these models. We can conclude that at a depth of about 10 km, the shear wave velocity is about 3.6 km/sec with a range from 3.57 to 3.7 km/sec. The estimated ground motion is not sensitive to this small variation of shear wave velocity at focal depth. In this study, we used a value of 3.6 km/sec for the shear wave velocity at the focal depth. For the density of rock at focal depth, we used  $\rho = 2.75 \text{ g/cm}^3$ .

For this study, our bedrock is the top of Paleozoic rocks. To evaluate the amplification, we also need to determine the velocity of Paleozoic rocks. In the Mississippi Embayment, there are some variations of shear wave velocity in the part close to ground surface. For down to the bottom of sediment (about 0.7 km depth), shear wave velocities vary from 0.56 to 2.1 km/sec. The low shear wave velocity layers in both Chiu et al. (1992) and Andrews et al. (1985) may be the shear wave velocity for sediment in the Mississippi Embayment not for Paleozoic rocks. In this study, we uses 2.1 km/sec as the shear wave velocity for the bedrock — top of Paleozoic rocks (Saikia et al., 1992) because it was based on observations in the West Tennessee. Toro et al. (1992) used a value of 2.4 km/sec as the shear wave velocity of Paleozoic rock at depth about 0.7 km.

**Table 2.1. Crustal Models for the New Madrid Region**

Base Depth (km)	Thickness (km)	$V_s$ (km/sec)	Density (gm/cm <sup>3</sup> )
Nuttli et al. (1969)			
1.0	1.0	1.60	
1.5	0.5	2.10	
2.0	0.5	3.28	
20.0	18.0	3.60	
40.0	20.0	3.92	
Andrews et al. (1984)			
0.65	0.65	0.56	
2.50	1.85	3.40	
5.00	2.50	2.80	
17.0	12.00	3.60	
27.0	10.00	3.80	
40.0	13.00	4.35	
Chiu et al. (1992)			
0.65	0.65	0.60	
2.50	1.85	3.56	
5.00	2.50	3.20	
17.0	12.00	3.57	
27.0	10.00	3.80	
40.0	13.00	4.20	
Saikia et al. (1992)			
0.50	0.50	2.10	2.20
1.50	1.00	3.28	2.50
9.50	8.00	3.60	2.70
19.50	10.00	3.70	2.90
39.50	20.00	4.20	3.00

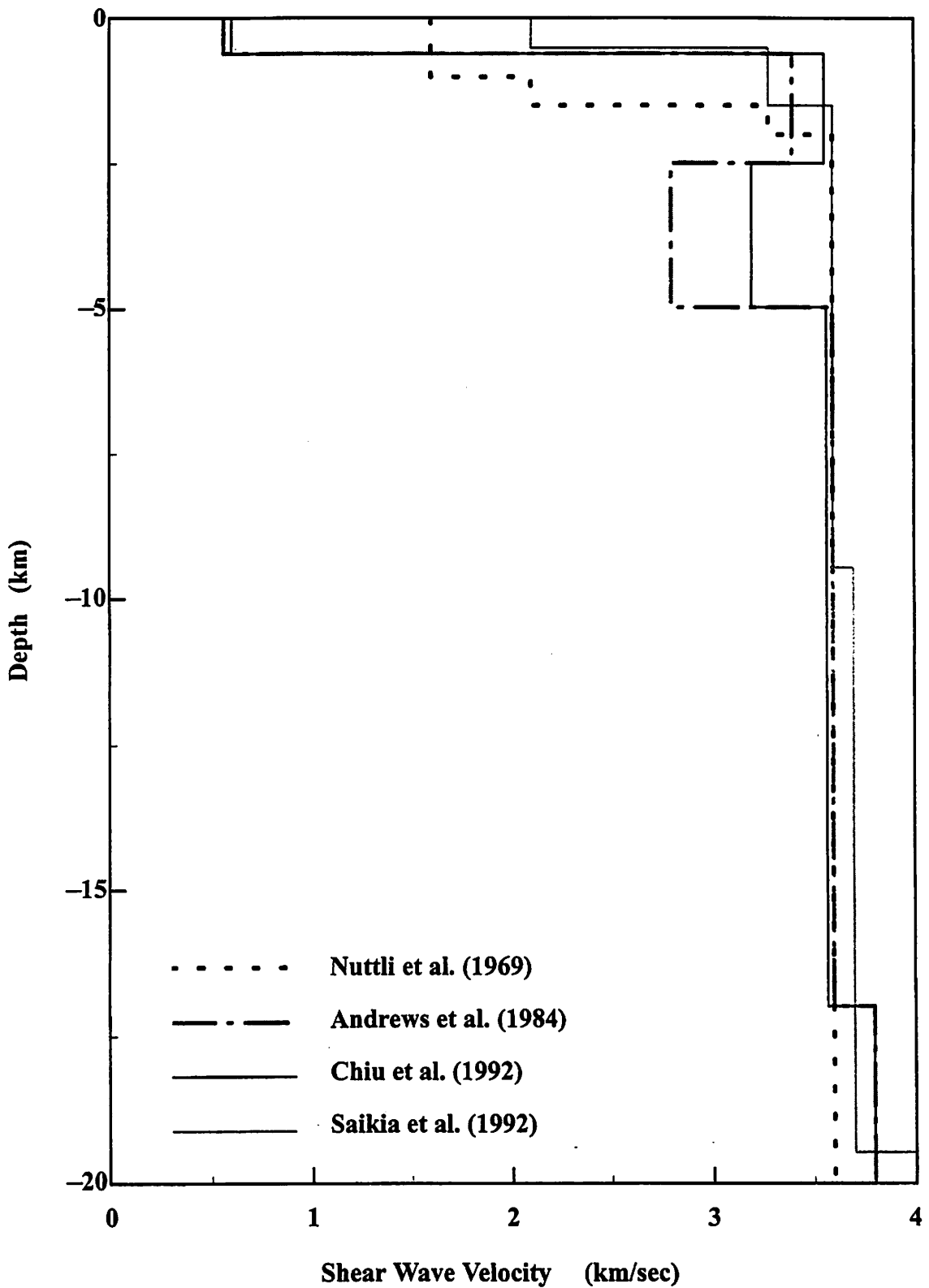


Figure 2.18. Comparison of Shear Wave Velocity of Upper Crust.

As it can be observed from Table 2.1 and Figure 2.18, there is no detailed information about the variation of shear wave velocity in Paleozoic rocks. Thus, it is impossible to determine the frequency dependent amplification factor from these crustal structures. In applications to the hard rock of eastern North America, most researchers (Boore and Atkinson, 1987; McGuire et al., 1988; and EPRI, 1993) did not consider the amplification because of small velocity gradients in ENA. However, Boore et al. (1996) considered the amplification of hard rock in the central and eastern North America. In this study, we adopted amplification factors from Boore et al. (1996).

**Table 2.2. Near Site Amplification Factors (Boore et al., 1996)**

$f$ (Hz)	0.1000	0.4079	0.8524	1.6300	3.5600	7.0250	13.950
$Am(f)$	1.000	1.074	1.120	1.154	1.177	1.187	1.193

## 2.6 Duration of Ground Motion

Another important factor in the estimation of ground motion is duration. Duration determines the distribution of seismic energy in the time domain because the assumption ground motion process is a stationary random process.

### 2.6.1 Factors Affecting Duration

There are two major factors which affect the duration of ground motion: (1) the seismic source and (2) the path of seismic wave propagation.

It is well known that the size of an earthquake is strongly correlated with dimensions of the seismic source zone or the length of the fault. Because the velocity of rupture propagation is limited, the longer the fault, the longer the time is needed to break the whole fault. Consequently, the duration of earthquake ground motion increases with the increase of earthquake magnitude.

The earth is made of rock layers with different properties. There are reflection, refraction, and scattering when the seismic wave travels from the seismic source to the receiver. Seismic waves may change from receiver to receiver owing to the difference of epicentral distance. Therefore, duration varies from site to site in ground motion observations.

### 2.6.2 Estimation of Duration

Following Herrmann (1985), we can write the duration of ground motion as

$$D = D_s + bR \quad (2.31)$$

where  $R$  is the hypocentral distance and  $D_s$  is the duration due to seismic source which is given by the inverse of the corner frequency (Hanks and McGuire, 1981)

$$D_s = \frac{1}{f_c} \quad (2.32)$$

and  $b$  is a constant to consider the path duration. Although different researchers may take different values of  $b$ , most researchers (Herrmann, 1985 and Boore et al., 1996) used  $b = 0.05$ . We also used  $b = 0.05$  in this study.